nature ecology & evolution

ARTICLES

https://doi.org/10.1038/s41559-021-01391-6

Neanderthals and *Homo sapiens* had similar auditory and speech capacities

Mercedes Conde-Valverde[1]✉, Ignacio Martínez[1,2], Rolf M. Quam[1,2,3,4], Manuel Rosa[1,5], Alex D. Velez[3], Carlos Lorenzo[6,7], Pilar Jarabo[5], José María Bermúdez de Castro[8,9], Eudald Carbonell[6,7,10] and Juan Luis Arsuaga[2,11]

The study of audition in fossil hominins is of great interest given its relationship with intraspecific vocal communication. While the auditory capacities have been studied in early hominins and in the Middle Pleistocene Sima de los Huesos hominins, less is known about the hearing abilities of the Neanderthals. Here, we provide a detailed approach to their auditory capacities. Relying on computerized tomography scans and a comprehensive model from the field of auditory bioengineering, we have established sound power transmission through the outer and middle ear and calculated the occupied bandwidth in Neanderthals. The occupied bandwidth is directly related to the efficiency of the vocal communication system of a species. Our results show that the occupied bandwidth of Neanderthals was greater than the Sima de los Huesos hominins and similar to extant humans, implying that Neanderthals evolved the auditory capacities to support a vocal communication system as efficient as modern human speech.

The linguistic capacities in Neanderthals have long been an area of active research and debate among palaeoanthropologists, albeit with little resolution[1–3]. The last two decades have seen increasing archaeological discoveries documenting complex behaviours in Neanderthals. These have been linked to the possible presence of language in Neanderthals, since it seems reasonable to suggest that such behaviours require the presence of a complex and efficient oral communication system[3]. Nevertheless, a different point of view maintains that the distinctive features of human language, absent in other organisms, include a symbolic element as well as a recursive syntactic process called 'merge'[4]. This latter process, at its simplest, uses two syntactic elements and assembles them to form a set and is argued to be exclusive to *Homo sapiens* and to have appeared no earlier than 100 kyr (refs. [1,4]).

Tracing the presence of symbolism and syntactic processes in the course of human evolution currently lies outside the realm of possibility in palaeontology[1]. Nevertheless, the study of human fossils can prove key to determining whether past human species, and in particular the Neanderthals, possessed the anatomy necessary to produce and perceive an oral communication system as complex and efficient as human speech, the usual (but not exclusive) vehicle for language. In other words, although palaeontology cannot study the evolution of the 'software' of language it can contribute to our understanding of the evolution of the 'hardware' of speech. In our opinion, to suggest that a past human species, such as the Neanderthals, may have had language, it is not only necessary to establish the presence of symbolism, which can be approached in the archaeological record[1] but also to demonstrate the existence of the anatomical bases necessary to produce and perceive articulated speech.

The study of brain endocasts has been one of the classic approaches to interpreting the cognitive and linguistic capacities in Neanderthals. Although the Neanderthals as a species are as encephalised as *H. sapiens*[5,6], clear differences have been documented in the cerebral organisation[7–9] as well as the allometric trajectories in both phylogenetic[10] and ontogenetic[11] terms. Nevertheless, the significance of these differences for inferring cognitive and linguistic capacities in Neanderthals remains actively debated[2,4,8,9,12,13].

During the last five decades, much debate has centred on whether the supralaryngeal vocal tract in Neanderthals was capable of producing the fundamental sounds of human speech[2]. While this debate remains unresolved, recent anatomical[14–16] and genetic[17] data support the idea that Neanderthals could have produced a wide repertoire of acoustic signals, facilitating a complex form of vocal communication. In this context, it would be particularly interesting to establish whether the auditory capacities in Neanderthals were capable, or not, of supporting a vocal communication system as efficient as that of our own species.

The auditory capacities in Neanderthals have been indirectly approached through comparative studies of the dimensions and proportions of the ear ossicles[18] as well as the functional properties of the middle ear[19]. These studies found broad similarities between Neanderthals and modern humans in both aspects, suggesting that these similarities might imply similar hearing abilities as well. On the other hand, on the basis of a few features of the external and middle ear, Masali et al.[20] proposed that Neanderthals had a slightly higher best audible frequency than modern humans.

More recently, a comprehensive model, based on a large number of anatomical variables directly related to auditory physiology, has

[1]Cátedra de Otoacústica Evolutiva y Paleoantropología (HM Hospitales-Universidad de Alcalá), Departamento de Ciencias de la Vida, Universidad de Alcalá, Madrid, Spain. [2]Centro Mixto (UCM-ISCIII) de Evolución y Comportamiento Humanos, Madrid, Spain. [3]Department of Anthropology, Binghamton University (SUNY), Binghamton, NY, USA. [4]Division of Anthropology, American Museum of Natural History, New York, NY, USA. [5]Departamento de Teoría de la Señal y Comunicaciones, Escuela Politécnica Superior, Universidad de Alcalá, Alcalá de Henares, Spain. [6]Àrea de Prehistòria, Departament d'Història i Història de l'Art, Universitat Rovira i Virgili, Tarragona, Spain. [7]Institut Català de Paleoecologia Humana i Evolució Social, Tarragona, Spain. [8]Centro Nacional de Investigación sobre la Evolución Humana (CENIEH), Burgos, Spain. [9]Anthropology Department, University College London, London, UK. [10]Departamento de Historia, Geografía y Comunicación, Universidad de Burgos, Burgos, Spain. [11]Departamento de Geodinámica, Estratigrafía y Paleontología, Facultad de Ciencias Geológicas, Universidad Complutense de Madrid, Madrid, Spain. ✉e-mail: mercedes.conde@fgua.es

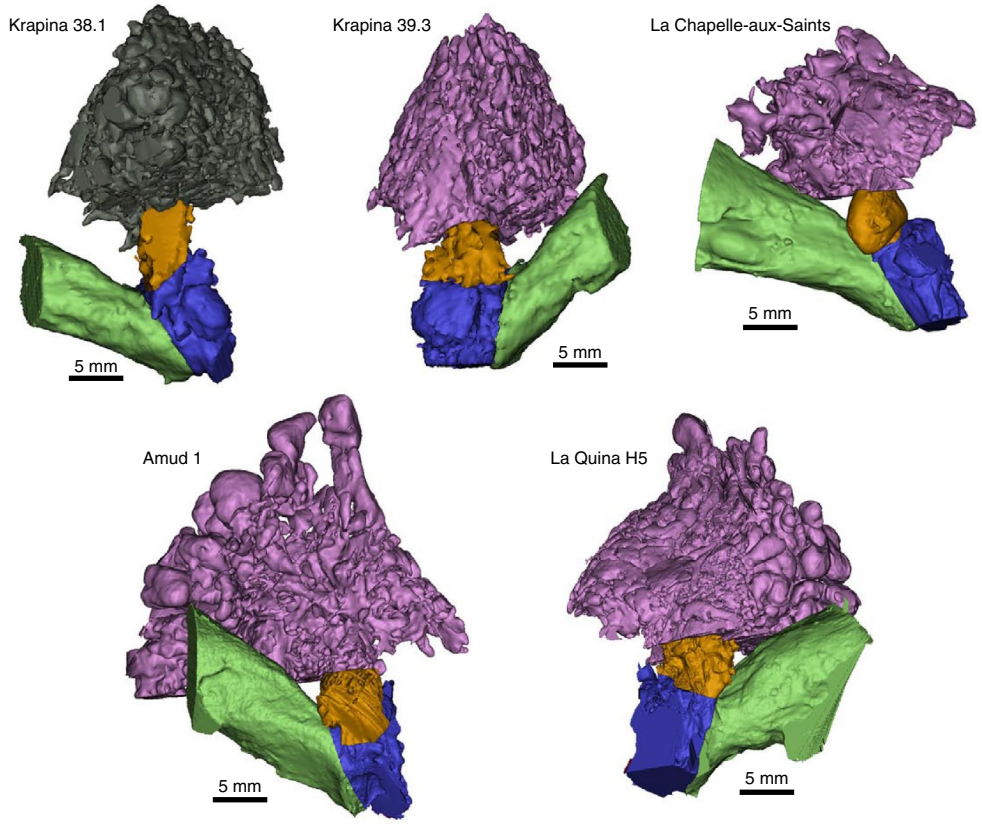

Fig. 1 | Anatomical reconstruction of the external and middle ear cavities in Neanderthals. External auditory canal (green), middle ear cavity (blue), aditus (orange) and mastoid air cells (purple/grey). Mastoid air cells of Krapina 38.1 (grey) are represented using the mastoid air cells of Krapina 39.3.

been used to estimate the sound power transmission (SPT) through the outer and middle ear in fossil hominins[14,21,22]. The SPT reflects the acoustic filtering process, leading to a frequency-dependent attenuation of sound power at the cochlear entrance, which largely shapes the resultant audiogram in living subjects[23]. The SPT directly depends on the dimensions of the different anatomical structures of the outer and middle ear[23], making it possible to estimate it in fossil species.

At the same time, on the basis of the SPT it is also possible to calculate the occupied bandwidth (OBW), defined as the width of a frequency band such that, below the lower and above the upper frequency limits, the mean powers are each equal to a specified percentage of the total mean power of a given signal spectrum[24]. In the present study, the OBW includes the range of frequencies which contains at least 90% of the sound power transmitted to the inner ear[14,21,22], reflecting the frequency range of maximum auditory sensitivity. The OBW is, in turn, directly related to the bandwidth of the oral communication channel. A wider communication channel bandwidth allows for a larger number of easily distinguishable acoustic signals to be used in the oral communication of a species. This improves the efficiency of communication (that is, the ability to deliver a clear message in the shortest amount of time) since it allows for an increase in the number of phonemes and a reduction of the perception error rate[25].

The theory of information, as outlined by Shannon[25], has been used to estimate the information rate of speech communication[26] and forms the basis for recent studies examining the correlation between speech intelligibility and bandwidth for people with normal and impaired hearing[27,28]. The influence of bandwidth reduction on speech intelligibility is reflected in the definition of the ANSI/ASA S3.5-1997 speech intelligibility index standard[29,30]. Thus, there is a clear link between the OBW and the oral communication system in humans.

Previous studies carried out on the European Middle Pleistocene fossils from the Sima de los Huesos (SH)[14,22] and in the early hominin taxa *Australopithecus africanus* and *Paranthropus robustus* from South Africa[21] showed that the OBW in the early hominins was quite similar to *Pan troglodytes*, while the SH fossils had an OBW more similar to, although somewhat narrower than, *H. sapiens*. In this context, establishing the OBW in Neanderthals would be particularly interesting. If this parameter is similar to that in the SH hominins, it could be argued that the Neanderthals developed more complex behaviours than their ancestors without the need to increase the efficiency of their communication system. Nevertheless, if the OBW in Neanderthals is wider than in the SH hominins, this would show that the increased behavioural complexity of the Neanderthals, compared with their ancestors, was accompanied by an increase in the efficiency of the oral communication system, suggesting a functional link between these two phenomena.

To establish the SPT and OBW in Neanderthals, we virtually reconstructed the outer and middle ear in five Neanderthal individuals (Fig. 1) from computerized tomography (CT) scans. We have also reconstructed the outer and middle ear in six new SH individuals and have carried out new reconstructions of three previously published individuals[14,21,22] on the basis of higher resolution CT scans (Extended Data Fig. 1). These data on the SH hominins are particularly relevant given their close phylogenetic relationship between the SH population and Neanderthals[5,31]. The fossil samples were compared with a sample of recent *H. sapiens* ($n=10$) published previously[21].

On the basis of anatomical measurements taken on the three-dimensional (3D) models (Extended Data Fig. 2 and

Table 1 | OBW values and exact test comparisons for *H. sapiens*, Neanderthals and SH hominins

	Lower limit (Hz)	Upper limit (Hz)	Bandwidth (Hz)
H. sapiens mean ± s.d.	813 ± 89	4,316 ± 367	3,503 ± 403
Range (n = 10)	660–1,010	3,815–5,000	2,980–4,340
Neanderthal mean ± s.d.	810 ± 78	4,035 ± 124	3,225 ± 187
Range (n = 5)	715–920	3,880–4,200	2,960–3,485
SH mean ± s.d.	758 ± 60	3,584 ± 242	2,826 ± 264
Range (n = 9)	635–820	3,170–3,965	2,400–3,265
Exact test			
SH versus Neanderthals	0.280	**0.004**	**0.012**
SH versus *H. sapiens*	0.150	**<0.001**	**0.001**
Neanderthals versus *H. sapiens*	0.929	0.196	0.206
Holm–Bonferroni corrected *P*			
SH versus Neanderthals	0.784	**0.028**	0.072
SH versus *H. sapiens*	0.750	**<0.001**	**0.008**
Neanderthals versus *H. sapiens*	0.929	0.784	0.784

For values in bold, $P < 0.05$.

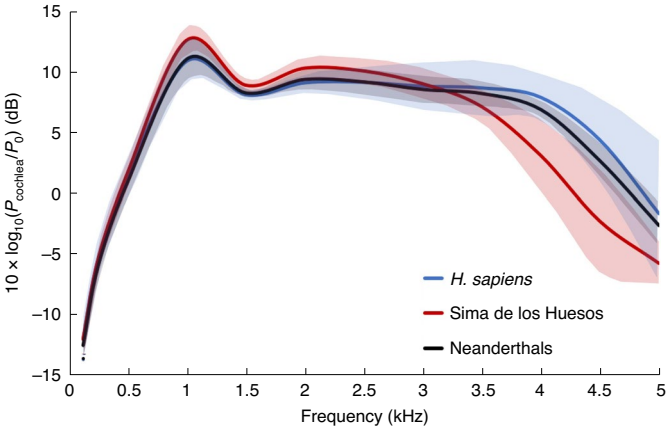

Fig. 2 | SPT in modern humans, the SH hominins and Neanderthals. Continuous lines represent the means and coloured areas show ±1 s.d.

Supplementary Table 1), we have calculated the SPT and OBW in the Neanderthals and the expanded SH sample (Table 1, Figs. 2 and 3, Extended Data Fig. 3 and Supplementary Table 2).

Results

Comparison with previous studies of the SH fossils. The auditory capacities in the SH fossils have been studied previously[14,22,32]. However, the SH sample used in the present study includes new data in several regards. First, the present study only includes complete individuals, where all the measurements of the outer and middle ear can be taken. Thus, two previously published incomplete individuals (AT-84 and AT-421), which relied on estimating the values for some missing variables[22], have been removed from the sample. In addition, previous studies on the auditory capacities of the SH hominins used medical CT scans for SH Crania (Cr.)3, Cr.5 and AT-1907 (ref. [22]). These same three individuals have now been CT scanned at a higher resolution, along with all the SH individuals included in this study (Cr.4, Cr.7, Cr.8, Cr.13, Cr.15 and Cr.16) (Supplementary Table 3). As a consequence, we carried out new reconstructions of the external and middle ear cavities of Cr.3, Cr.5 and AT-1907, using the new CT scans and obtained new values for the anatomical variables (Supplementary Table 1). The descriptive statistics of the anatomical variables and the SPT in seven SH individuals, relying on the new reconstructions, were published previously[32], but here we include the individual values for these variables in these same individuals, together with the unpublished values in Cr.16 (Supplementary Table 1 for anatomical variables and Supplementary Table 2 for SPT values). In addition, we provide here the individual values for the OBW, a central objective of the present study, for all the SH individuals on the basis of the higher resolution CT scans (Supplementary Table 2).

For Cr.3 and AT-1907, the differences between the previous anatomical measurements and the new values are very small (Supplementary Table 1) and the differences for SPT and OBW are also very small (Extended Data Fig. 4). In the case of Cr.5, the differences between the previously published values and the new data are greater, particularly for the variables L_{AD}, A_{TM}, L_{EAC} and A_{EAC} and the SPT and OBW have also been affected. In particular, the OBW in Cr.5 is narrower than previously published (Extended Data Fig. 4), although, importantly, the new value for OBW falls within the range of variation in the expanded SH sample.

The mean value for OBW in the enlarged SH sample is slightly lower than that previously published[22]. The new SH mean is still significantly higher than the mean OBW in *P. troglodytes* (Extended Data Fig. 5) but is significantly lower than that in modern humans (Table 1). This lower mean value is mainly due to the low values for OBW obtained in three new individuals included in this study: Cr.4, Cr.8 and Cr.13 (Supplementary Table 2). These are the three largest crania in the SH sample, on the basis of their cranial capacities (Supplementary Table 4). This relationship between cranial size and OBW is explained by the fact that the largest crania also tend to show the longest external auditory canals. Since the length of the external auditory canal is strongly negatively correlated with the OBW (Extended Data Fig. 6), the inclusion of the largest crania in the sample has lowered the mean OBW for the SH hominins. Given this relationship between cranial size and the OBW, it is important to emphasise that our Neanderthal comparative sample includes the smallest (La Quina H5) as well as two of the largest (La Chapelle-aux-Saints 1 and Amud 1) known Neanderthal crania (Supplementary Table 2).

Results in the Neanderthals. The results revealed no statistically significant differences between the Neanderthal and modern human means in any of the anatomical variables (Extended Data Fig. 7) or the SPT (Fig. 2 and Extended Data Fig. 3) or OBW (Table 1 and Fig. 3). Contrary to previous suggestions[20], our results for the SPT indicate a similar best frequency in Neanderthals and modern humans. More importantly, the OBW values for Neanderthals fall within the modern human range of variation, except for La Chapelle-aux-Saints 1, which is just below the lower limit of modern humans. At the same time, Neanderthals show some differences from the SH sample in a few anatomical variables (Extended Data Fig. 7), as well as the SPT at frequencies between 4 and 5 kHz (Fig. 2 and Extended Data Fig. 3) and the OBW, which is wider in Neanderthals (Table 1 and Fig. 3) and extended towards higher frequencies. These differences in the OBW can be explained by the significantly lower values in Neanderthals than in the SH sample for a few anatomical variables, including the volume of the aditus (V_{AD}), radius of the entrance of the aditus ($R_{AD(entrance)}$) and length of

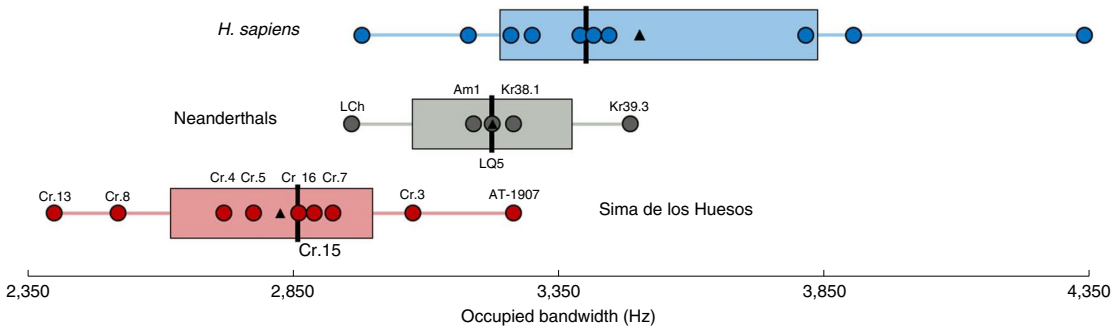

Fig. 3 | OBW in SH, Neanderthals and modern humans. Means (triangles), medians (vertical black bars), Q1 (25%) to Q3 (75%) (boxes) and individual values (circles). Cr, SH Crania; Kr, Krapina; LCh, La Chapelle-aux-Saints 1; Am1, Amud 1; LQ5, La Quina H5.

the external auditory canal (L_{EAC}), which show negative correlations (especially L_{EAC}) with the OBW (Extended Data Fig. 6).

Discussion and conclusions

Our results show that the auditory capacities in Neanderthals do not differ from those in modern humans, including the presence of an extended OBW in both species. Importantly, the OBW in Neanderthals extends towards frequencies that primarily involve consonant production[33], suggesting that this may have been an important component of their vocal communication, one that would distinguish them from the pattern of largely vowel-based vocal communication in chimpanzees[34] and, indeed, nearly all mammals[35]. Although much of the acoustic information in human speech is concentrated in the region up to ~2.5 kHz (for example, the first two formant frequencies of the vowels), the region of 3–5 kHz is associated with the production of high-frequency consonants[33]. Consonants in this frequency range mainly consist of the voiceless plosives (stops), such as those associated with the sounds corresponding to the English letters /t/ and /k/, and the voiceless fricatives, including those associated with the sounds corresponding to the English letters /f/, /s/ and /th/. While other consonants do occur at lower frequencies, the high-frequency consonants are particularly salient features in human speech. Voiceless plosives are present in over 90% of the world's languages, with /t/ and /k/ being the most strongly represented[36]. Similarly, fricative consonants are found in >90% of the world's languages and among the fricatives, /s/ is the most common voiceless fricative, present in >80% of languages, with /f/ also occurring at high frequencies[36]. Importantly, because these consonants are voiceless, they do not propagate across the landscape and are limited to short-range intraspecific communication. Indeed, voiceless consonants may represent "…the evolutionarily oldest group of consonants"[37].

In addition, there is evidence that vowels and consonants are processed separately in the human brain[38] and that the latter are particularly important for determining word meaning[39]. In modern human adults with age-related hearing loss, the high-frequency consonants are also the first to be affected, with a concomitant loss in intelligibility and comprehension[40], demonstrating a direct link between the OBW and language comprehension. This relationship between consonant production and an extended OBW helps make the link between audition and vocalisation explicit and helps explain how an extended OBW corresponds to a vocal communication system in Neanderthals that was as complex and efficient as human speech.

Compared to their evolutionary ancestors from the SH, the Neanderthals show an increase in both the OBW and behavioural complexity, including sophisticated subsistence strategies, such as the exploitation of a wide variety of resources[41–43], the systematic production and use of fire[44,45], the possible construction of musical instruments[46] and the expression of symbolic behaviours[47–50], including potential evidence for parietal art[51–53]. Importantly, this relationship between an increase in both behavioural complexity and the OBW was also found in previous studies of the auditory capacities in early hominins (*Australopithecus* and *Paranthropus*) and the SH hominins. The early hominins show an OBW that was similar to that in chimpanzees[21], while the SH hominins show an OBW that was considerably extended compared with the early hominins, along with an increase in behavioural complexity. This increased behavioural complexity in the SH hominins includes sophisticated stone tool manufacture (mode 2)[54], evidence of communal hunting of large game species[55], incipient mortuary practices[56] and conspecific care[57,58]. In our opinion, this is strong evidence in favour of the coevolution of increased behavioural complexity and increased efficiency in vocal communication throughout the course of human evolution.

The narrower OBW in the SH hominins, with respect to Neanderthals and modern humans, indicates that the increase in the OBW occurred in both Neanderthals and modern humans after their last common ancestor. This may have evolved through an evolutionary process of adaptive convergence for an increasingly efficient vocal communication system in both lineages. Alternatively, it could be attributed to potential gene flow between the two lineages. We would point out that the Krapina Neanderthals, who show an extended OBW similar to modern humans, date to ~130 thousand years ago (ka)[59] and predate the estimated earliest evidence of gene flow between these two species[60]. This would seem to reject the idea that the Neanderthals acquired their extended OBW through gene flow from modern humans. Nevertheless, it would still be possible that modern humans acquired their extended OBW through gene flow from the Neanderthals. Future study of the auditory capacities in early *H. sapiens* (older than 100 ka) can reject or reinforce this possibility. If the hypothesis of gene flow is rejected, then the only explanation for the extended OBW in both species would be an adaptive convergence for an increasingly efficient vocal communication system.

In summary, our results reinforce the idea that the Neanderthals possessed the same auditory capabilities as *H. sapiens* necessary to support a vocal communication system as complex and efficient as human speech. It is true that the presence of the anatomical 'hardware' necessary to produce human-like speech in the Neanderthals does not necessarily imply the presence of similar mental 'software' as in *H. sapiens* and, by implication, the presence of a language with the same characteristics as that of our own species[1]. Nevertheless, our results, together with recent discoveries indicating symbolic behaviours in Neanderthals, reinforce the idea that they possessed a type of human language, one that was very different in its complexity and efficiency from any other oral communication system used by non-human organisms on the planet.

Methods

Fossil specimens. *SH sample (Spain).* The site is dated to a minimum of 430 kyr and the SH fossils represent early ancestors of the later Neanderthals[5,32]. Cranium 3 is a very complete calvarium belonging to an adolescent[5], preserving both temporal bones. In this study we have used the left one (AT-4103) because it is the best preserved. Cranium 4 is a complete neurocranium belonging to an adult[61] preserving both temporal bones. This specimen suffered from a bilateral exostosis in both external auditory canals and was considered to have suffered conductive hearing loss[62]. Nevertheless, a more recent and thorough study demonstrated that the exostoses did not modify the auditory pattern of this individual[32] and so it can be used in this study. We have used the right side because it is slightly better preserved. Cranium 5 is a complete adult skull preserving both temporal bones, the right malleus (AT-666) and the left stapes (AT-667)[61]. For this study we have used the left temporal bone because it is better preserved. Cranium 7 is a very complete calvarium of a young adult individual preserving both temporal bones[5]. We have used the left temporal bone (AT-804) because it is complete. Cranium 8 is most of the left side of a calvaria of an adult individual, including the temporal bone (AT-433)[5]. Cranium 13 is a very complete calvarium of an adult individual preserving the right temporal bone (AT-2872 and AT-2873). Cranium 15 is a very complete skull of an adult individual which includes the complete right temporal bone (AT-5528). Cranium 16 is the partial cranium of a late adolescent which preserve both temporal bones. In this study, the left temporal bone (AT-6969) was used because it is the most complete one. AT-1907 is the isolated right temporal bone of a late adolescent individual with the associated malleus (AT-3746) and incus (AT-3747)[21]. AT-5518 is an isolated stapes associated with temporal bone AT-5500.

The bony structures of the outer and middle ear (including the tympanic cavity and the ear ossicles) are completely ossified and fully formed at birth[63] and the external auditory canal reaches adult size by the age of 9 yr in modern humans[64]. Thus, all the bony structures included in the present study have already reached their adult dimensions before adolescence in our own species, justifying the inclusion of adolescent individuals in this study.

Neanderthal sample. The Krapina sample (Croatia) site is dated to around 130 kyr (ref. [59]). Two specimens have been included in this study: the adult right temporal bone Kr.38.1 (Tp.2) and the late adolescent left temporal bone Kr39.3 (Tp.4) (ref. [65]). Amud 1 (Israel) is a very complete skull of an adult individual[66], including the complete left temporal bone. The age-estimates for the Mousterian levels of Amud Cave range from 50 to 70 kyr (ref. [67]) and the level where the Amud 1 cranium was found has been dated to 53 ± 8 kyr (ref. [68]). La Chapelle-aux-Saint 1 (France) is a very complete skull of an adult individual[69] and the right temporal bone was used in this study. The site has been estimated to date between 47 and 56 kyr (ref. [70]). La Quina H5 (France) is a very complete calvarium of an adult individual which preserves the left temporal bone[71]. The site of La Quina has been dated to ~48–42.5 kyr (ref. [72]).

CT parameters. The Neanderthals and the SH fossils were CT scanned at different institutions and at different resolutions (Supplementary Table 3). The CT scans for the Krapina Neanderthals (Kr.39.3 and Kr.38.1) were downloaded from the NESPOS platform and the resolution is lower than that for the other fossil specimens. To ensure the accuracy of our measurements in these individuals, we have compared our values for the A_{OW}, A_{TM} and the distance between the centre of the tympanic groove and the centre of the oval window in Kr.39.3 with the values previously published[19], which were taken on microCT images. Our values for these variables are very similar to those published in ref. [19], indicating that our measurements in this individual were not affected by the lower resolution of the CT scans.

Segmentation process and anatomical measurements. Virtual reconstructions and metric data collection were performed using the Mimics v.18 software following the standard procedure established in previous works[15,21,22]. We performed semi-automatic segmentation relying on the half-maximum-height thresholding protocol[73] to establish the boundary between the temporal bone and the air-filled cavities. This boundary was calculated as the average between the threshold for the external auditory canal and that of the mastoid air cells. Manual segmentation was necessary in the middle ear cavity of the specimen Krapina 39.3 since it was broken. In the case of Krapina 38.1, it was not possible to segment the mastoid air cells because they were filled with sediment. The anatomical measurements used to calculate the SPT have been defined in refs. [15,21,22] and are defined in Extended Data Figs. 8 and 9. Most of the measures necessary for estimating the SPT were taken on the 3D models using Mimics. However, the areas of the entry and exit of the aditus ad antrum, the cross-sectional area of the external auditory canal and the area of the oval window were measured in two-dimensional images with Photoshop v.5 (Extended Data Fig. 8).

Calculation of the SPT and OBW. The use of electrical circuits to model mechanical and acoustic systems is well known in acoustic engineering[74]. This approach has been used by several researchers to develop electrical circuit models of the outer and middle ear[75,76], which constitutes the basis of the model used in the present study. This model is a slightly modified version[21] of the model published in ref. [76], to take into account more recent knowledge found in the literature. The electrical circuit which models the acoustic and mechanical behaviour of the external and middle ear is built with two-port sections described with 'transmission matrices'[77], to make the implementation with MATLAB R2019a easier. This comprehensive model is used to estimate the SPT through the outer and middle ear as described below.

- The concha is modelled as an exponential horn. The smaller cross-sectional area is equivalent to the cross-sectional area of the ear canal.
- The ear canal is modelled as a tube with constant cross-sectional area.
- The middle ear cavity is modelled in the same way as that proposed in previous works[21,75,76]. The compliance of the tympanic air space located directly behind the tympanic membrane is modelled with a capacitor, which is connected in parallel to the equivalent electrical circuit of a Helmholtz resonator representing the aditus ad antrum and the mastoid air cell cavities, composed of a capacitor, representing the compliance of the mastoid air cells, a resistance and an inertance, representing the aditus ad antrum. These parameters are calculated from physical measurements. For modelling purposes, we have considered the entrance to the epitympanum as representing the entrance to the aditus ad antrum and the exit into the mastoid antrum as representing the exit from the aditus ad antrum (Extended Data Fig. 8). Subsequently, we have calculated the radius of the neck of the resonator as the average between the radii at both extremes (entrance and exit) of the aditus ad antrum. The overall middle ear cavity model is connected in a series branch and is an antiresonant circuit, which gives rise to a notch at the antiresonant frequency, which depends on the physical parameters.
- No modifications have been introduced in the tympanic membrane–malleus network, which is the same as that used in previous works[21,75,76].
- The ossicular chain is modelled with a series branch composed of a resistance, compliance and mass, that jointly model the mass of the malleus and incus, the compliance and damping with the supporting ligaments. After that, a transformer is included and the transformer parameter is the ratio of the malleus–incus functional lengths. A shunt branch is connected to the transformer, with a capacitor and a resistor, that accounts for the loss of stapes velocity from compression of the ossicular joints. The ossicular chain model is completed with the mass of the stapes, and another transformer, whose parameter is the stapes footplate area.
- Finally, the model is completed by the annular ligament block, where no modifications have been introduced compared to Rosowski's model and the cochlear input impedance (Z_c). The cochlear input impedance has been considered resistive, taking into account the cochlear input impedance measurements in 11 human cadaver ears published by Aibara and colleagues[78], who found a flat, resistive cochlear input impedance with an average value of 21.1 GΩ from 0.1 to 5.0 kHz.

The reliability of this model was assessed in ref. [21] by comparing the theoretical middle ear pressure gain obtained for modern humans with those measured experimentally in ref. [78], finding no significant differences.

The electrical parameters used in the model are associated with anatomical structures of the ear[22]. Some of these parameters are related with skeletal structures accessible in fossils, while others are related with soft tissues, which are not preserved in fossil specimens. The respective value for modern humans[76,78] has been used for the soft tissue-related variables which cannot be measured in fossil specimens. The use of modern human values for the soft tissue-related variables may introduce a bias in the results for the SPT (as well as the OBW) in the fossil specimens. However, previous studies[14,21,22] have shown that the use of these same modern human values for the soft tissue variables to model the auditory capacities in chimpanzees does not make the resultant SPT more human-like. Rather, the SPT results are fully compatible with the empirical audiogram-based results in chimpanzees[14,21,22]. Thus, it is reasonable to conclude that the use of modern human soft tissue values does not bias the SPT results in the fossil specimens towards modern humans.

This model, where each block is modelled with transmission parameters, makes it possible to calculate the sound power at the entrance to the cochlea, assuming an incident plane wave of constant intensity stimulating the auditory system. The sound power at the entrance to the cochlea is calculated using the stapes velocity and the cochlear impedance. The results for SPT presented in this paper are calculated for an incident plane wave intensity of $I = 1 \times 10^{-12}$ W m^{-2} and are presented in dB relative to $P_0 = 1 \times 10^{-18}$ W.

The bandwidth of the external and middle ear, considered as a communication channel, is directly related to the channel capacity, an indicator of the amount of information that can be transmitted through the channel with arbitrarily low error rate. For real channels, there are different definitions of channel bandwidth that could be considered, which could provide slightly different values but are equally useful when used for comparative purposes. In this paper, we have relied on the OBW[79], defined as the bandwidth such that under the lower cutoff frequency and above the upper cutoff frequency, the average power is equal to a specified percentage, $\beta/2$, of the total average power. In this paper, $\beta/2$ is considered as equal

to 5%, such that the OBW includes the range of frequencies which contains at least 90% of the sound power transmitted to the inner ear.

Statistical analysis. To test for statistical differences between samples we relied on the exact test and we have performed a Holm–Bonferroni correction for *P* values for the OBW comparisons. All statistical analyses were carried out using the Past 4.02 software package.

Reporting Summary. Further information on research design is available in the Nature Research Reporting Summary linked to this article.

Data availability

All the technical data regarding the CT scans as well as the measurements of 3D reconstructions necessary to reproduce our work are offered within the manuscript and Supplementary Information. CT scans of fossil material from Krapina are available at the Nespos platform. CT scans of the fossil specimens La Chapelle-aux-Saints 1 and La Quina H5 are the property of Musée de l'Homme (France); that for Amud 1 is the property of Tel Aviv University (Israel); and the fossil specimens from the Sima de los Huesos are property of Junta de Castilla y León (Spain), to whom application must be made for access. Interested readers may contact the authors, who will assist in getting in touch with the relevant institutions. The CT scans and 3D models of recent *H. sapiens* are available at Morphosource (https://www.morphosource.org/projects/000343670?locale=en).

Received: 15 August 2020; Accepted: 12 January 2021;
Published online: 01 March 2021

References

1. Tattersall, I. The material record and the antiquity of language. *Neurosci. Biobehav. Rev.* **81**, 247–254 (2017).
2. Albessard-Ball, L. & Balzeau, A. Of tongues and men: a review of morphological evidence for the evolution of language. *J. Lang. Evol.* **3**, 79–89 (2018).
3. Dediu, D. & Levinson, S. C. Neanderthal language revisited: not only us. *Curr. Opin. Behav. Sci.* **21**, 49–55 (2018).
4. Bolhuis, J. J., Tattersall, I., Chomsky, N. & Berwick, R. C. How could language have evolved? *PLoS Biol.* **12**, e1001934 (2014).
5. Arsuaga, J. L. et al. Neandertal roots: cranial and chronological evidence from Sima de los Huesos. *Science* **344**, 1358–1363 (2014).
6. Arsuaga, J. L. et al. Postcranial morphology of the Middle Pleistocene humans from Sima de los Huesos, Spain. *Proc. Natl Acad. Sci. USA* **112**, 11524–11529 (2015).
7. Balzeau, A., Holloway, R. L. & Grimaud-Hervé, D. Variations and asymmetries in regional brain surface in the genus *Homo*. *J. Hum. Evol.* **62**, 696–706 (2012).
8. Pearce, E., Stringer, C. & Dunbar, R. I. New insights into differences in brain organization between Neandertals and anatomically modern humans. *Proc. R. Soc. B* **280**, 20130168 (2013).
9. Neubauer, S., Hublin, J. J. & Gunz, P. The evolution of modern human brain shape. *Sci. Adv.* **4**, eaao5961 (2018).
10. Bruner, E., Manzi, G. & Arsuaga, J. L. Encephalization and allometric trajectories in the genus *Homo*: evidence from the Neandertal and modern lineages. *Proc. Natl Acad. Sci. USA* **100**, 15335–15340 (2003).
11. Zollikofer, C. P. E. & Ponce de León, M. S. Pandora's growing box: inferring the evolution and development of hominin brains from endocasts. *Evol. Anthropol.* **22**, 20–33 (2013).
12. Balzeau, A., Gilissen, E., Holloway, R. L., Prima, S. & Grimaud-Hervé, D. Variations in size, shape and asymmetries of the third frontal convolution in hominids: paleoneurological implications for hominin evolution and the origin of language. *J. Hum. Evol.* **76**, 116–128 (2014).
13. Marie, D. et al. Left brain asymmetry of the planum temporale in a nonhominid primate: redefining the origin of brain specialization for language. *Cereb. Cortex* **28**, 1808–1815 (2018).
14. Martínez, I. et al. Communicative capacities in Middle Pleistocene humans from the Sierra de Atapuerca in Spain. *Quat. Int.* **295**, 94–101 (2013).
15. Boë, L. J., Heim, J. L., Honda, K. & Maeda, S. The potential Neandertal vowel space was as large as that of modern humans. *J. Phon.* **30**, 465–484 (2002).
16. de Boer, B. Loss of air sacs improved hominin speech abilities. *J. Hum. Evol.* **62**, 1–6 (2012).
17. Krause, J. et al. The derived FOXP2 variant of modern humans was shared with Neandertals. *Curr. Biol.* **17**, 1908–1912 (2007).
18. Quam, R. M., Martínez, I. & Arsuaga, J. L. Reassessment of the La Ferrassie 3 Neandertal ossicular chain. *J. Hum. Evol.* **64**, 250–262 (2013).
19. Stoessel, A. et al. Morphology and function of Neandertal and modern human ear ossicles. *Proc. Natl Acad. Sci. USA* **113**, 11489–11494 (2016).
20. Masali, M., Maffei, M. & Borgognini Tarli, S. M. in *Circeo 1. The Neandertal Skull: Studies and Documentation* (eds Piperno, M. & Scichilone, G.) 321–338 (Instituto Poligrafico e Zecca Dello Stato, 1991).
21. Quam, R. et al. Early hominin auditory capacities. *Sci. Adv.* **1**, e1500355 (2015).
22. Martínez, I. et al. Auditory capacities in Middle Pleistocene humans from the Sierra de Atapuerca in Spain. *Proc. Natl Acad. Sci. USA* **101**, 9976–9981 (2004).
23. Rosowski, J. The effects of external and middle ear filtering on auditory threshold and noise-induced hearing loss. *J. Acoust. Soc. Am.* **90**, 124–135 (1991).
24. International Telecommunication Union. *Recommendation ITU-R SM.443-4, Bandwidth Measurement at Monitoring Stations* (SM Series Spectrum Management, 2007).
25. Shannon, C. E. A mathematical theory of communication. *Bell Syst. Tech. J.* **27**, 379–423 (1948) .
26. Fano, R. M. The information theory point of view in speech communication. *J. Acoust. Soc. Am.* **22**, 691–696 (1950).
27. Letowski, T. R. & Scharine, A. A. *Correlation Analysis of Speech Intelligibility and Metrics for Speech Transmission* (US Army Research Laboratory, 2017).
28. Skinner, M. W. & Miller, J. D. Amplification bandwidth and intelligibility of speech in quiet and noise for listeners with sensorineural hearing loss. *Audiology* **22**, 253–279 (1983).
29. Kates, J. M. & Arehart, K. H. Coherence and the speech intelligibility index. *J. Acoust. Soc. Am.* **117**, 2224–2237 (2005).
30. *Methods for Calculation of the Speech Intelligibility Index* ANSI/ASA S3.5-1997 (ANSI, reaffirmed 2020).
31. Meyer, M. et al. Nuclear DNA sequences from the Middle Pleistocene Sima de los Huesos hominins. *Nature* **531**, 504–507 (2016).
32. Conde-Valverde, M. et al. A revision of the conductive hearing loss in Cranium 4 from the Middle Pleistocene site of Sima de los Huesos (Burgos, Spain). *J. Hum. Evol.* **135**, 102663 (2019).
33. Fant, C. G. M. *Speech Sounds and Features* (MIT Press, 1973).
34. Mitani, J. C., Hunley, K. L. & Murdoch, M. E. Geographic variation in the calls of wild chimpanzees: a reassessment. *Am. J. Primatol.* **47**, 133–151 (1999).
35. Lieberman, P. *On the Origins of Language: An Introduction to the Evolution of Human Speech* (Macmillan, 1975).
36. Maddieson, I. *Patterns of Sounds* (Cambridge Univ. Press, 1984).
37. Lameira, A. R., Maddieson, I. & Zuberbühler, K. Primate feedstock for the evolution of consonants. *Trends Cogn. Sci.* **18**, 60–62 (2014).
38. Caramazza, A., Chialant, D., Capasso, R. & Miceli, G. Separable processing of consonants and vowels. *Nature* **403**, 428–430 (2000).
39. Owren, M. & Cardillo, G. The relative roles of vowels and consonants in discriminating talker identity versus word meaning. *J. Acoust. Soc. Am.* **119**, 1727–1739 (2006).
40. Divenyi, P. L., Stark, P. B. & Haupt, K. M. Decline of speech understanding and auditory thresholds in the elderly. *J. Acoust. Soc. Am.* **118**, 1089–1100 (2005).
41. Weyrich, L. S. et al. Neanderthal behaviour, diet, and disease inferred from ancient DNA in dental calculus. *Nature* **544**, 357–361 (2017).
42. Krueger, K. L. et al. Anterior dental microwear textures show habitat-driven variability in Neandertal behavior. *J. Hum. Evol.* **105**, 13–23 (2017).
43. Zilhão, J. et al. Last Interglacial Iberian Neandertals as fisher-hunter-gatherers. *Science* **367**, eaaz7943 (2020).
44. Heyes, P. J. et al. Selection and use of manganese dioxide by Neanderthals. *Sci. Rep.* **6**, 22159 (2016).
45. Vallverdú, J. et al. Combustion structures of archaeological level O and Mousterian activity areas with use of fire at the Abric Romaní rockshelter (NE Iberian Peninsula). *Quat. Int.* **247**, 313–324 (2012).
46. Tuniz, C. et al. Did Neanderthals play music? X-ray computed micro-tomography of the Divje babe 'flute'. *Archaeometry* **54**, 581–590 (2012).
47. Rendu, W. et al. Evidence supporting an intentional Neandertal burial at La Chapelle-aux-Saints. *Proc. Natl Acad. Sci. USA* **111**, 81–86 (2014).
48. Radovčić, D., Sršen, A. O., Radovčić, J. & Frayer, D. W. Evidence for Neandertal jewelry: modified white-tailed eagle claws at Krapina. *PLoS ONE* **10**, e0119802 (2015).
49. Jaubert, J. et al. Early Neanderthal constructions deep in Bruniquel cave in southwestern France. *Nature* **534**, 111–114 (2016).
50. Hoffmann, D. L., Angelucci, D. E., Villaverde, V., Zapata, J. & Zilhão, J. Symbolic use of marine shells and mineral pigments by Iberian Neandertals 115,000 years ago. *Sci. Adv.* **4**, eaar5255 (2018).
51. Hoffmann, D. L. et al. U-Th dating of carbonate crusts reveals Neandertal origin of Iberian cave art. *Science* **359**, 912–915 (2018).
52. Pearce, D. G. & Bonneau, A. Trouble on the dating scene. *Nat. Ecol. Evol.* **2**, 925–926 (2018).
53. Hoffmann, D. L. et al. Dates for Neanderthal art and symbolic behaviour are reliable. *Nat. Ecol. Evol.* **2**, 1044–1045 (2018).
54. Carbonell, E. et al. Les premiers comportements funéraires auraient-ils pris place à Atapuerca, il y a 350 000 ans? *L'Anthropologie* **107**, 1–14 (2003).
55. Rodriguez-Hidalgo, A. et al. Human predatory behavior and the social implications of communal hunting based on evidence from the TD10. 2 bison bone bed at Gran Dolina (Atapuerca, Spain). *J. Hum. Evol.* **105**, 89–122 (2017).

56. Sala, N. et al. Lethal interpersonal violence in the Middle Pleistocene. *PLoS ONE* **10**, e0126589 (2015).
57. Gracia, A. et al. Craniosynostosis in the Middle Pleistocene human Cranium 14 from the Sima de los Huesos, Atapuerca, Spain. *Proc. Natl Acad. Sci. USA* **106**, 6573–6578 (2009).
58. Bonmatí, A. et al. Middle Pleistocene lower back and pelvis from an aged human individual from the Sima de los Huesos site, Spain. *Proc. Natl Acad. Sci. USA* **107**, 18386–18391 (2010).
59. Rink, W. J., Schwarcz, H. P., Smith, F. H. & Radovčić, J. ESR ages for Krapina hominids. *Nature* **378**, 24 (1995).
60. Sankararaman, S., Patterson, N., Li, H., Pääbo, S. & Reich, D. The date of interbreeding between Neandertals and modern humans. *PLoS Genet.* **8**, e1002947 (2012).
61. Arsuaga, J. L., Martínez, I., Gracia, A., Carretero, J. M. & Carbonell, E. Three new human skulls from the Sima de los Huesos Middle Pleistocene site in Sierra de Atapuerca, Spain. *Nature* **362**, 534–537 (1993).
62. Pérez, P. J., Gracia, A., Martínez, I. & Arsuaga, J. L. Paleopathological evidence of the cranial remains from the Sima de los Huesos Middle Pleistocene site (Sierra de Atapuerca, Spain). Description and preliminary inferences. *J. Hum. Evol.* **33**, 409–421 (1997).
63. Quam, R. *Temporal Bone Anatomy and the Evolution of Acoustic Capacities in Fossil Humans*. PhD thesis, State University of New York (2006).
64. Wright, C. G. Development of the human external ear. *J. Am. Acad. Audiol.* **8**, 379–382 (1997).
65. Radovčić, J., Smith, F., Trinkaus, E. & Wolpoff. M. H. *The Krapina Hominids. An Illustrated Catalog of Skeletal Collection* (Croatian Natural History Museum, 1988).
66. Endo, B. & Kimura, T. in *The Amud Man and his Cave Site* (eds Suzuki, H. & Takai, F.) 231–406 (Univ. Tokyo Press, 1970).
67. Valladas, H. et al. TL dates for the Neanderthal site of the Amud cave, Israel. *J. Archaeol. Sci.* **26**, 259–268 (1999).
68. Rink, W. et al. Electron spin resonance (ESR) and thermal ionization mass spectrometric (TIMS) $^{230}Th/^{234}U$ dating of teeth in Middle Paleolithic layers at Amud Cave, Israel. *Geoarchaeology* **16**, 701–717 (2001).
69. Boule, M. L'Homme fossile de La Chapelle-aux-Saints. *Ann. Paleontol.* **6**, 111–172 (1911).
70. Grün, R. & Stringer, C. B. Electron spin resonance dating and the evolution of modern humans. *Archaeometry* **33**, 153–199 (1991).
71. Martin, H. *L'Homme Fossile de La Quina* (Gaston Doin, 1923).
72. Higham, T. et al. The timing and spatiotemporal patterning of Neanderthal disappearance. *Nature* **512**, 306–309 (2014).
73. Coleman, M. N. & Colbert, M. W. Technical note: CT thresholding protocols for taking measurements on three-dimensional models. *Am. J. Phys. Anthropol.* **133**, 723–725 (2007).
74. Harris, R. W. Electromechanical analogies in acoustics. *Appl. Acoust.* **3**, 265–281 (1970).
75. Kringlebotn, M. Network model for the human middle ear. *Scand. Audiol.* **17**, 75–85 (1988).
76. Rosowski, J. J. in *Auditory Computation* (eds Hawkins, H. L. et al.) 15–61 (Springer, 1996).
77. Lampton, M. Transmission matrices in electroacoustics. *Acta Acust. United Acust.* **39**, 239–251 (1978).
78. Aibara, R., Welsh, J. T., Puria, S. & Goode, R. L. Human middle-ear sound transfer function and cochlear input impedance. *Hear. Res.* **152**, 100–109 (2001).
79. *Radiocommunication Vocabulary* ITU-R V.573e4 (International Telecommunication Union, 2007).

Acknowledgements

We thank the following individuals and institutions for providing access to fossils and specimens housed in their care: A. Balzeau (Musée de l'Homme, France) and I. Hershkovitz and J. Abramov (Tel Aviv University, Israel). CT scanning of the SH fossils was carried out at the Laboratorio de Evolución Humana (Burgos, Spain) by R. García and L. Rodríguez. Financial support for this study was provided by the Ministerio de Ciencia, Innovación y Universidades (PGC2018-093925-B-C33) of the Spanish Government. This project forms part of the Bioacústica Evolutiva y Paleoantropología research group of Universidad de Alcalá. M.C.-V. received a predoctoral grant from the Fundación Atapuerca. R.M.Q. received financial support from Binghamton University and the Ginés de los Ríos grant programme from the Universidad de Alcalá. A.D.V. received financial support from Binghamton University and the Fulbright Commission.

Author contributions

M.C.-V., I.M., R.M.Q. and M.R. designed the research and wrote the article. M.C.-V., A.D.V. and C.L. reconstructed the 3D models for the study and collected data on the 3D models. M.R. and P.J. modelled the hearing results. J.M.B.C., E.C. and J.L.A. provided critical comments and directed the excavation and the research project at the Atapuerca sites.

Competing interests

The authors declare no competing interests.

Additional information

Extended data is available for this paper at https://doi.org/10.1038/s41559-021-01391-6.

Supplementary information The online version contains supplementary material available at https://doi.org/10.1038/s41559-021-01391-6.

Correspondence and requests for materials should be addressed to M.C.-V.

Peer review information *Nature Ecology & Evolution* thanks Amelie Beaudet and the other, anonymous, reviewer(s) for their contribution to the peer review of this work. Peer reviewer reports are available.

Reprints and permissions information is available at www.nature.com/reprints.

Publisher's note Springer Nature remains neutral with regard to jurisdictional claims in published maps and institutional affiliations.

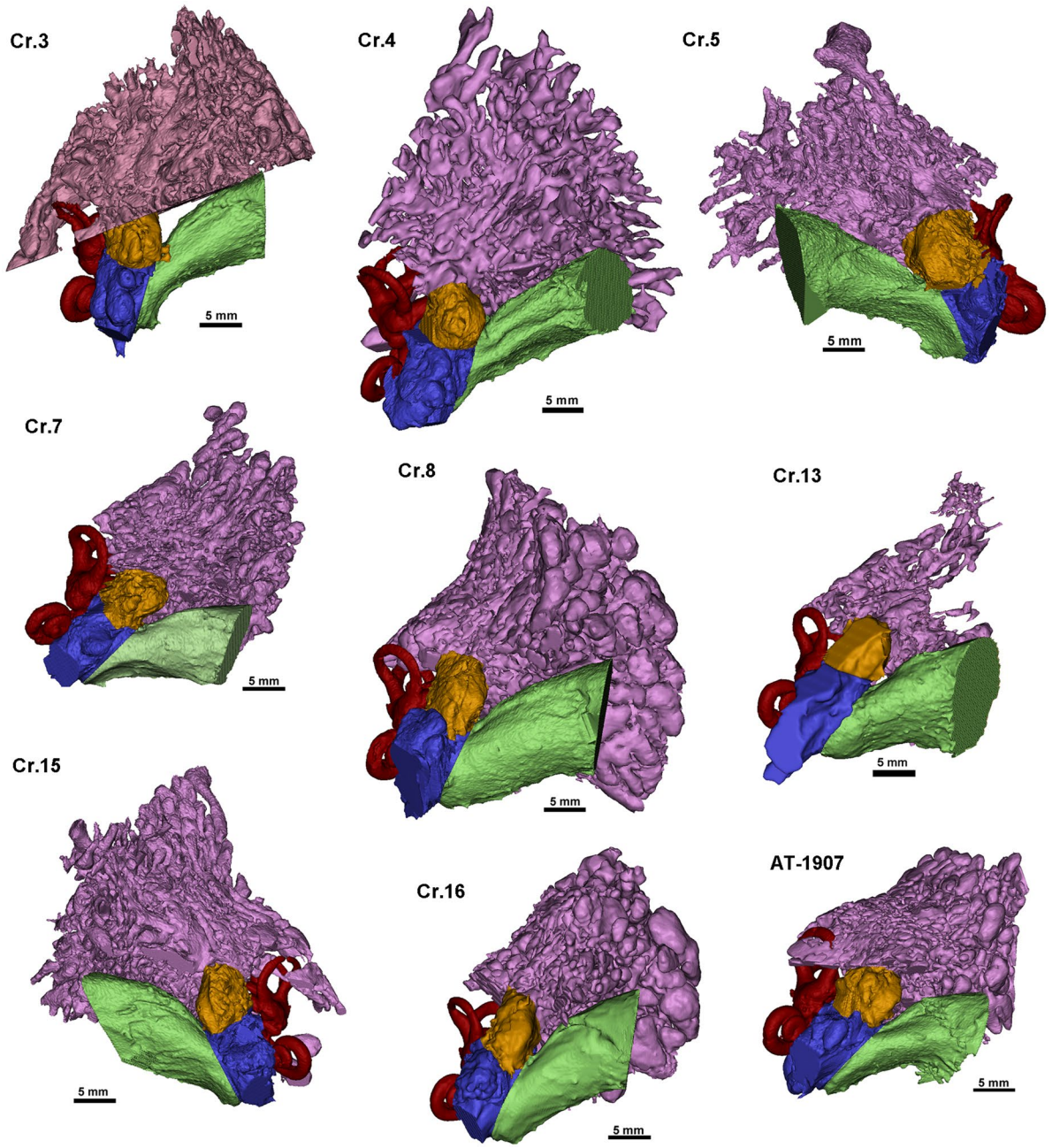

Extended Data Fig. 1 | 3D models of the external, middle and inner ear of the Sima de los Huesos fossils. External auditory canal (green), middle ear cavity (blue), *aditus* (orange) and mastoid air cells (purple), inner ear (red).

	H. sapiens		Neanderthals		Sima de los Huesos	
	Mean ± s.d.	**Range (*n*)**	**Mean ± s.d.**	**Range (*n*)**	**Mean ± s.d.**	**Range (*n*)**
V_{AD} (cm^3)	0.12 ± 0.02	0.09–0.17 (10)	0.13 ± 0.01	0.11–0.15 (5)	0.20 ± 0.03	0.15–0.25 (9)
V_{MA} (cm^3)	4.43 ± 2.27	0.52–8.02 (10)	2.85 ± 1.33	1.20–4.34 (4)	3.88 ± 2.19	0.98–8.78 (9)
V_{MEC} (cm^3)	0.46 ± 0.09	0.33 – 0.62 (10)	0.49 ± 0.06	0.38–0.53 (5)	0.60 ± 0.09	0.45–0.72 (9)
L_{AD} (mm)	4.35 ± 0.70	3.70–6.25 (10)	4.42 ± 0.29	4.09–4.80 (5)	5.24 ± 0.83	3.88–6.58 (9)
$R_{AD(exit)}$ (mm)	2.42 ± 0.24	2.01–2.73 (10)	2.54 ± 0.24	2.24–2.82 (4)	2.87 ± 0.26	2.49–3.25 (9)
$R_{AD(entrance)}$ (mm)	2.96 ± 0.13	2.80–3.21 (10)	3.08 ± 0.24	2.66–3.27 (5)	3.33 ± 0.16	3.11–3.59 (9)
$L_{EAC\ (Comp)}$ (mm)	21.00 ± 1.98	17.70–23.76 (10)	22.97 ± 1.65	20.36–24.87 (5)	26.33 ± 2.07	22.61–28.92 (9)
A_{TM} (mm^2)	65.06 ± 5.51	56.61–74.00 (10)	70.99 ± 3.18	66.77–73.90 (5)	72.34 ± 4.21	65.55–79.12 (9)
A_{EAC} (mm^2)	37.1 ± 6.91	29.05–51.04 (10)	36.13 ± 1.53	34.42–38.59 (5)	39.4 ± 12.1	22.79–62.24 (8)
A_{OW} (mm^2)	3.53 ± 0.56	2.54–4.37(10)	3.17 ± 0.43	2.59–3.79 (5)	3.05 ± 0.55	2.34–3.94 (8)
A_{FP} (mm^2)	2.92 ± 0.21	2.5–3.13 (7)	2.85 ± 0.39	2.33–3.41 (5)	2.74 ± 0.46	2.11–3.55 (9)
L_M/L_I	1.26 ± 0.08	1.2–1.4 (7)	1.17 ± 0.09	1.05-1.25 (6)	1.19*	(1)
M_M+M_I (mg)	49.2 ± 4.4	41.3–53.0 (8)	52.7†		52.7†	(1)
M_S (mg)	2.5 ± 0.6	1.4–3.2 (8)	2.3‡		2.3‡	1.89-2.70 (2)

Extended Data Fig. 2 | Anatomical variables used to calculate the sound power transmission in the SH and Neanderthal individuals. V_{AD} = Volume of *aditus*; V_{MA} = Volume of mastoid air cells; V_{MEC} = Volume of tympanic cavity; L_{AD} = Length of *aditus*; $R_{AD(exit)}$ = Radius of *aditus* exit; $R_{AD(entrance)}$ = Radius of *aditus* entrance; $L_{EAC\ (Comp)}$ = Complete length of external auditory canal; A_{TM} = Area of tympanic membrane; A_{EAC} = Cross-sectional area of the external auditory canal; A_{OW} = Area of oval window; A_{FP} = Area of stapes footplate; L_M/L_I = Malleus/incus lever ratio; $M_M + M_I$ = Mass of malleus + incus; M_S = Mass of stapes. *L_M/L_I for SH calculated from the malleus (AT-3746) and the incus (AT-3747) belonging to the temporal bone AT-1907[21]. †$M_M + M_I$ for SH was calculated from the malleus (AT-3746) and the incus (AT-3747) belonging to the temporal bone AT-1907[22]. The same value has been used for the Neanderthals. ‡M_S: the values of Cr. 5 and AT-5518 have been measured directly, and the mean value of both specimens have been used for the rest of the SH and Neanderthal samples.

	0.125 kHz (dB)	0.25 kHz (dB)	0.5 kHz (dB)	1 kHz (dB)	1.5 kHz (dB)	2 kHz (dB)	2.5 kHz (dB)	3 kHz (dB)	3.5 kHz (dB)	4 kHz (dB)	4.5 kHz (dB)	5 kHz (dB)
H. sapiens mean ± SD	-12.0 ± 1.8	-5.5 ± 1.7	1.4 ± 1.7	10.9 ± 1.7	8.1 ± 0.5	9.1 ± 0.8	9.2 ± 1.4	8.8 ± 1.9	8.7 ± 2.3	7.9 ± 2.0	4.4 ± 3.5	-1.7 ± 5.8
Range (*n* = 10)	-16.6– -10.6	-10.0– -4.2	-3.2 – 2.7	6.3–12.3	7.3–8.7	7.6–10.0	6.5–10.8	5.2–11.2	4.3–11.4	4.5–10.3	-2.1–10.5	-11.6–5.3
Neanderthal mean ± SD	-12.6 ± 1.1	-6.1 ± 1.1	0.9 ± 1.2	11.1 ± 1.7	8.3 ± 0.3	9.4 ± 0.8	9.2 ± 1.0	8.6 ± 1.1	8.3 ± 1.0	6.9 ± 0.7	2.7 ± 1.4	-2.6 ± 1.8
Range (*n* = 5)	-14.3– -11.5	-7.9– -5.0	-1.1–2.0	8.6–12.6	8.0–8.7	8.5–10.6	8.0–10.8	7.0–9.8	6.5–9.2	6.0–7.6	1.2–4.7	-5.04–0.4
SH mean ± SD	-12.1 ± 1.1	-5.5 ± 1.1	1.7 ± 1.1	12.6 ± 1.0	8.9 ± 0.5	10.3 ± 0.9	10.1 ± 1.0	9.0 ± 1.3	7.1 ± 1.4	3.1 ± 2.9	-2.3 ± 4.2	-5.8 ± 1.7
Range (*n* = 9)	-14.5– -10.9	-7.9– -4.3	-0.4–3.3	11.0–14.4	8.0–9.7	8.7–11.3	8.0–11.1	7.1–10.5	4.2–8.7	-3.2–6.7	-12.7–1.54	-8.4– -3.9
Exact test												
SH vs Neanderthals	0.364	0.381	0.298	0.083	0.060	0.104	0.112	0.381	0.147	**0.004**	**0.004**	**0.012**
SH vs *H. sapiens*	0.435	0.484	0.842	**0.010**	**0.008**	**0.013**	0.069	0.842	0.113	**< 0.001**	**0.001**	0.095
Neanderthals vs *H. sapiens*	0.164	0.174	0.310	0.768	0.882	0.837	0.859	0.859	0.768	0.371	0.164	0.440

Extended Data Fig. 3 | Sound power transmission (SPT) values and Exact test comparisons for H. sapiens, Neanderthals and SH. Sound power transmission (SPT) at the entrance to the cochlea relative to $P_0 = 10^{-18}$ W for an incident plane wave intensity of 10^{-12} W/m^2. In bold $P < 0.05$.

		Previously published[21]			This study		
		Cr3	Cr5	AT1907	Cr3	Cr5	AT1907
Occupied Bandwidth	Lower limit (Hz)	715	730	735	725	795	700
	Upper limit (Hz)	3845	4095	3990	3800	3570	3965
	Bandwidth (Hz)	3130	3365	3255	3075	2775	3265
Sound Power Transmission (SPT)	0.5 kHz (dB)	1.89	0.04	1.27	1.99	0.86	2.47
	1 kHz (dB)	12.96	12.1	12.13	13	11.75	13.58
	1.5 kHz (dB)	8.01	7.58	8.03	8.51	9.39	7.99
	2 kHz (dB)	8.97	7.89	8.89	9.58	10.98	8.67
	2.5 kHz (dB)	8.41	6.48	8.23	9.27	10.96	8.02
	3 kHz (dB)	7.76	5.3	7.31	8.54	9.74	7.19
	3.5 kHz (dB)	7.51	5.34	6.94	7.86	7.53	7.19
	4 kHz (dB)	5.55	5.65	6.23	5.43	3.6	6.68
	4.5 kHz (dB)	0.74	0.3	2.47	0.73	-0.98	1.54
	5 kHz (dB)	-4.16	-8.54	-2.99	-3.94	-5.03	-5.16

Extended Data Fig. 4 | Comparison between values previously published and the present study for the occupied bandwidth and sound power transmission in three SH individuals. Sound power transmission (SPT) at the entrance to the cochlea relative to $P_0 = 10^{-18}$ W for an incident plane wave intensity of 10^{-12} W/m^2.

		P. troglodytes vs SH	*P. troglodytes* vs Neanderthals	*P. troglodytes* vs *H. sapiens*
Occupied Bandwidth	Lower limit (Hz)	**<0.001**	**<0.001**	**<0.001**
	Upper limit (Hz)	**<0.001**	**<0.001**	**<0.001**
	Bandwidth (Hz)	**0.005**	**<0.001**	**<0.001**
Sound Power Transmission (SPT)	0.125 kHz (dB)	0.053	**0.013**	0.223
	0.25 kHz (dB)	**0.002**	**0.005**	**0.013**
	0.5 kHz (dB)	**<0.001**	**<0.001**	**<0.001**
	1 kHz (dB)	0.269	0.509	0.251
	1.5 kHz (dB)	**<0.001**	**0.009**	**0.002**
	2 kHz (dB)	**<0.001**	**0.036**	**0.043**
	2.5 kHz (dB)	**0.001**	0.115	**0.029**
	3 kHz (dB)	**<0.001**	**0.001**	**0.001**
	3.5 kHz (dB)	**<0.001**	**<0.001**	**<0.001**
	4 kHz (dB)	**<0.001**	**<0.001**	**<0.001**
	4.5 kHz (dB)	**0.001**	**<0.001**	**<0.001**
	5 kHz (dB)	0.111	**0.027**	**0.002**

Extended Data Fig. 5 | Results of the Exact test for the occupied bandwidth and sound power transmission between *P. troglodytes* and the SH sample. Previous data for *P. troglodytes* sample[21]. Sound power transmission (SPT) at the entrance to the cochlea was calculated relative to $P_0 = 10^{-18}$ W for an incident plane wave intensity of 10^{-12} W/m^2. In bold $P < 0.05$.

		V_{AD} (cm^3)	V_{MA} (cm^3)	V_{MEC} (cm^3)	L_{AD} (mm)	$R_{AD(exit)}$ (mm)	$R_{AD(entrance)}$ (mm)	$L_{EAC\ (Comp)}$ (mm)	A_{TM} (mm^2)	A_{EAC} (mm^2)	A_{FP} (mm^2)
OBW	r	**-0.652**	-0.178	**-0.513**	**-0.579**	-0.172	**-0.595**	**-0.940**	-0.100	-0.292	0.131
	P	**0.001**	0.934	**0.010**	**0.003**	0.422	**0.002**	**<0.001**	0.644	0.166	0.542

Extended Data Fig. 6 | Correlations between the occupied bandwidth and anatomical variables calculated on the pooled modern human, SH and Neanderthal sample. OBW = Occupied bandwidth; V_{AD} = Volume of *aditus*; V_{MA} = Volume of mastoid air cells; V_{MEC} = Volume of tympanic cavity; L_{AD} = Length of *aditus*; $R_{AD(exit)}$ = Radius of *aditus* exit; $R_{AD(entrance)}$ = Radius of *aditus* entrance; $L_{EAC\ (Comp)}$ = Complete length of external auditory canal; A_{TM} = Area of tympanic membrane; A_{EAC} = Cross-sectional area of the external auditory canal; A_{FP} = Area of stapes footplate. In bold $P < 0.05$.

	V_{AD} (cm^3)	V_{MA} (cm^3)	V_{MEC} (cm^3)	L_{AD} (mm)	$R_{AD(exit)}$ (mm)	$R_{AD(entrance)}$ (mm)	$L_{EAC\ (Comp)}$ (mm)	A_{TM} (mm^2)	A_{EAC} (mm^2)	A_{FP} (mm^2)
SH vs Neanderthals	**0.002**	0.505	**0.025**	0.042	0.106	**0.046**	**0.019**	0.699	0.606	0.797
SH vs *H. sapiens*	**<0.001**	0.661	**0.004**	**0.028**	**0.002**	**<0.001**	**<0.001**	**0.010**	0.661	0.410
Neanderthals vs *H. sapiens*	0.271	0.240	0.322	0.533	0.394	0.173	0.099	0.075	0.859	0.530

Extended Data Fig. 7 | Results of the Exact test for the anatomical variables in the *H. sapiens*, SH and Neanderthal samples. V_{AD} = Volume of *aditus*; V_{MA} = Volume of mastoid air cells; V_{MEC} = Volume of tympanic cavity; L_{AD} = Length of *aditus*; $R_{AD(exit)}$ = Radius of *aditus* exit; $R_{AD(entrance)}$ = Radius of *aditus* entrance; $L_{EAC\ (Comp)}$ = Complete length of external auditory canal; A_{TM} = Area of tympanic membrane; A_{EAC} = Cross-sectional area of the external auditory canal; A_{FP} = Area of stapes footplate. In bold $P < 0.05$.

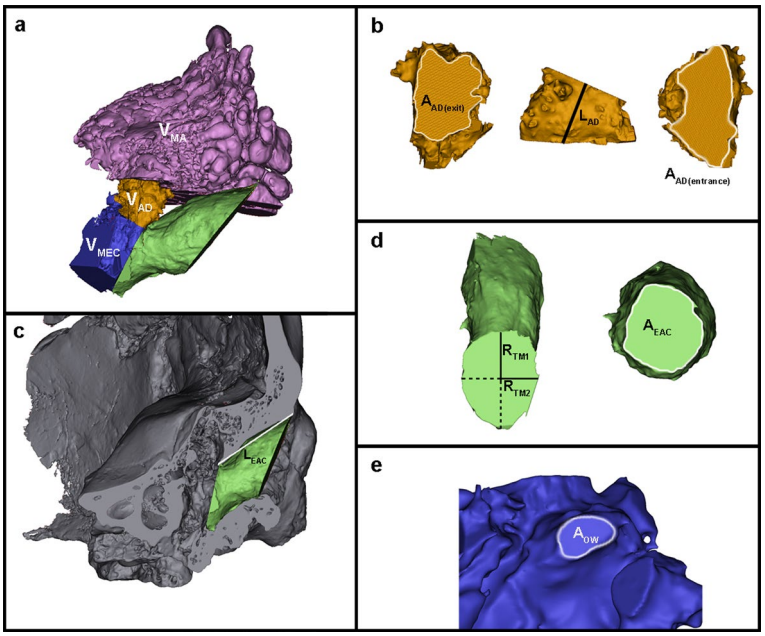

Extended Data Fig. 8 | 3D model of the external and middle ear cavities of La QuinaH5 showing the measurement of the variables used to estimate the sound power transmission through the outer and middle ear. a, Complete 3D model of the ear structures showing the volumes of the mastoid air cells (V_{MA}), of the aditus (V_{AD}) and of the middle ear cavity (V_{MEC}). **b**, 3D model of the *aditus ad antrum* showing measurement of the aditus exit ($A_{AD(exit)}$), length (L_{AD}) and entrance ($A_{AD(entrance)}$). **c**, 3D model of the temporal bone and external auditory canal (EAC) showing the measurement of the length of the bony EAC (L_{EAC}). **d**, 3D model of the EAC showing measurement of the size of the tympanic membrane (R_{TM1} and R_{TM2}) and cross-section of the EAC (A_{EAC}). **e**, 3D model of the oval window showing the measurement of the area (A_{OW}). See Extended Data Fig. 9 for measurement definitions.

Measurement (unit)	Definition	Extended Data
V_{AD} (mm^3)	Volumen of the *aditus ad antrum*.	Fig. 8a
V_{MA} (mm^3)	Volume of the the mastoid air cells.	Fig. 8a
V_{MEC} (mm^3)	Volume of the tympanic cavity, limited by the plane that coincides with the tympanic sulcus and by the entrance plane to the *aditus ad antrum*.	Fig. 8a
$A_{AD(entrance)}$ (mm^2)	Area of the entrance to the *aditus ad antrum* from the middle ear cavity.	Fig. 8b
$R_{AD(entrance)}$ (mm)	Radius of the entrance to the *aditus ad antrum* from the middle ear cavity calculated as the radius of a circle whose area is equal to $A_{AD(entrance)}$.	
$A_{AD(exit)}$ (mm^2)	Area of the exit from the *aditus ad antrum* to the mastoid air cells.	Fig. 8b
$R_{AD(exit)}$ (mm)	Radius of the exit from the *aditus ad antrum* to the mastoid air cells calculated as the radius of a circle whose area is equal to $A_{AD(exit)}$.	
L_{AD} (mm)	Length of *aditus ad antrum*. Measured from the central point of the *aditus ad antrum* entrance to the central point of the *aditus ad antrum* exit.	Fig. 8b
$L_{EAC(comp)}$ (mm)	Length of the complete cartilaginous external auditory canal (EAC). To include the exclusively cartilaginous lateral portion of the EAC we have calculated it by multiplying the length of the bony EAC by a factor of 1.5 (*6*).	Fig. 8c
R_{TM1} (mm)	Half of the greater diameter of the tympanic membrane, measured in the tympanic sulcus.	Fig. 8d
R_{TM2} (mm)	Half the lesser diameter of the tympanic membrane, measured in the tympanic sulcus perpendicular to the R_{TM1}.	Fig. 8d
A_{TM} (mm^2)	Tympanic membrane area calculated as an ellipse of radii R_{TM1} and R_{TM2}.	
A_{EAC} (mm^2)	Area of the cross-section of the EAC. Measured at the most posterosuperior point of the tympanic sulcus and perpendicular to an axis between the central point of the tympanic membrane and the central point of the external acoustic meatus.	Fig. 8d
A_{OW} (mm^2)	Area of the oval window.	Fig. 8e
A_{FP} (mm^2)	Area of the stapes footplate.	
$M_M + M_I$ (mg)	Combined mass of the malleus and incus.	
L_M (mm)	Functional length of the malleus measured as the maximum length between the tip of the lateral process and the tip of the manubrium.	
L_I (mm)	Functional length of the incus, measured as the length between the most anteroinferior point of the articular facet and the tip of the long process with the bone oriented in the axis of rotation.	
L_M/L_I	Ratio between the functional lengths of the malleus and the incus (Middle Ear Lever Ratio).	
M_S (mg)	Mass of the stapes.	

Extended Data Fig. 9 | Definition of the anatomical measurements used to calculate the sound powertransmission through the outer and middle ears. Definitions published before in refs. [15,21,22].

nature research

Corresponding author(s): Mercedes Conde-Valverde

Last updated by author(s): Dec 18, 2020

Reporting Summary

Nature Research wishes to improve the reproducibility of the work that we publish. This form provides structure for consistency and transparency in reporting. For further information on Nature Research policies, see our Editorial Policies and the Editorial Policy Checklist.

Statistics

For all statistical analyses, confirm that the following items are present in the figure legend, table legend, main text, or Methods section.

n/a	Confirmed	
☐	☒	The exact sample size (*n*) for each experimental group/condition, given as a discrete number and unit of measurement
☐	☒	A statement on whether measurements were taken from distinct samples or whether the same sample was measured repeatedly
☐	☒	The statistical test(s) used AND whether they are one- or two-sided *Only common tests should be described solely by name; describe more complex techniques in the Methods section.*
☒	☐	A description of all covariates tested
☒	☐	A description of any assumptions or corrections, such as tests of normality and adjustment for multiple comparisons
☐	☒	A full description of the statistical parameters including central tendency (e.g. means) or other basic estimates (e.g. regression coefficient) AND variation (e.g. standard deviation) or associated estimates of uncertainty (e.g. confidence intervals)
☐	☒	For null hypothesis testing, the test statistic (e.g. *F*, *t*, *r*) with confidence intervals, effect sizes, degrees of freedom and *P* value noted *Give P values as exact values whenever suitable.*
☒	☐	For Bayesian analysis, information on the choice of priors and Markov chain Monte Carlo settings
☒	☐	For hierarchical and complex designs, identification of the appropriate level for tests and full reporting of outcomes
☒	☐	Estimates of effect sizes (e.g. Cohen's *d*, Pearson's *r*), indicating how they were calculated

Our web collection on statistics for biologists contains articles on many of the points above.

Software and code

Policy information about availability of computer code

Data collection	Sima de los Huesos CT-Scan: YXLON Compact (YXLON International X-Ray) industrial multislice computed tomography (CT) scanner; Krapina CT-Scan: SIEMENS/Sensation 16; Amud 1 CT-Scan: Diondo d3 high-resolution micro-CT system; La Chapelle-aux-Saints 1 and La Quina H5 CT-Scan: Phoenix x|ray v|tome|x L 240-180 microCT scanner.
Data analysis	Mimics v.18 Past 4.02 MATLAB R2019a

For manuscripts utilizing custom algorithms or software that are central to the research but not yet described in published literature, software must be made available to editors and reviewers. We strongly encourage code deposition in a community repository (e.g. GitHub). See the Nature Research guidelines for submitting code & software for further information.

Data

Policy information about availability of data

All manuscripts must include a data availability statement. This statement should provide the following information, where applicable:

- Accession codes, unique identifiers, or web links for publicly available datasets
- A list of figures that have associated raw data
- A description of any restrictions on data availability

The authors declare that the main data supporting the findings of this study are available within the article and its Supplementary Information files. Extra data are available from the corresponding author upon request.

Field-specific reporting

Please select the one below that is the best fit for your research. If you are not sure, read the appropriate sections before making your selection.

☐ Life sciences ☐ Behavioural & social sciences ☒ Ecological, evolutionary & environmental sciences

For a reference copy of the document with all sections, see nature.com/documents/nr-reporting-summary-flat.pdf

Ecological, evolutionary & environmental sciences study design

All studies must disclose on these points even when the disclosure is negative.

Study description	This study calculates the sound power transmission and occupied bandwidth of 5 Neandertals and 9 specimens from the Middle pleistocene site Sima de los Huesos. The results were compared with a reference sample of 10 modern humans.
Research sample	We used original fossil material 9 individuals from Sima de los Huesos. We have used CT-scans of 5 Neandertals: three of them available from the institutions were they are housed (Musée de l'Homme: La Chapelle-aux-Saint1 and La Quina H5; Tel-Aviv University: Amud 1) and another two from Nespos (Krapina 38.1 and 39.3). Modern humans data from published references.
Sampling strategy	Our sampling strategy was based on availability of fossil materials of Sima de los Huesos (N=9), CT scans of Neandertal specimens (N=5), and published data of modern humans.
Data collection	3D reconstructions of the ear cavities were produced by MCV, ADV and CL. Linear measurements were taken by MCV, IM, RMQ, ADV and CL. Sound power transmission and occupied bandwidth were calculated by MR and PJ.
Timing and spatial scale	3D reconstructions of the ear cavities were made from 2018 to 2020, linear measurements were taken and processed in 2019-2020 and sound power transmission and occupied bandwidth were calculated in 2020.
Data exclusions	No data were excluded.
Reproducibility	All the data and procedures needed to reproduce our results are available in the manuscript, extended data and supplementary material. Any other related information in order to reproduce our results could be required to the corresponding author.
Randomization	All the specimens have been classified according to the species to which they belong (Homo sapiens, Homo neanderthalensis) except in the case of the fossils of the Sima de los Huesos, which have been grouped in an independent sample.
Blinding	*Describe the extent of blinding used during data acquisition and analysis. If blinding was not possible, describe why OR explain why blinding was not relevant to your study.*

Did the study involve field work? ☐ Yes ☒ No

Reporting for specific materials, systems and methods

We require information from authors about some types of materials, experimental systems and methods used in many studies. Here, indicate whether each material, system or method listed is relevant to your study. If you are not sure if a list item applies to your research, read the appropriate section before selecting a response.

Materials & experimental systems

n/a	Involved in the study
☒	☐ Antibodies
☒	☐ Eukaryotic cell lines
☐	☒ Palaeontology and archaeology
☒	☐ Animals and other organisms
☒	☐ Human research participants
☒	☐ Clinical data
☒	☐ Dual use research of concern

Methods

n/a	Involved in the study
☒	☐ ChIP-seq
☒	☐ Flow cytometry
☒	☐ MRI-based neuroimaging

Palaeontology and Archaeology

Specimen provenance	The fossils of Sima de los Huesos were CT scanned by Dr. R. García and Dr. L. Rodríguez with the permission of Dr. J. L. Arsuaga. The CT scans of La Chapelle aux Saints and La Quina H5 were provided by Dr. A. Balzeau (Musée de l'Homme, France), and CT scan of Amud 1 was provided by Dr. I. Hershkovitz and Dr. J. Abramov (Tel Aviv University, Israel). The Krapina Neandertals used are available in Nespos platform (www.nespos.org).
Specimen deposition	The CT scans of La Chapelle aux Saints and La Quina H5 are housed at Musée de l'Homme (Paris, France), CT scan of Amud 1 is

Specimen deposition	housed at Tel Aviv University (Israel). CT scans of Krapina Neandertal individuals are stored in Nespos platform. Junta de Castilla y León (Spain) is the repository of the Sima de los Huesos fossils.
Dating methods	No new dates are provided.

☐ Tick this box to confirm that the raw and calibrated dates are available in the paper or in Supplementary Information.

Ethics oversight	No ethical approval was required.

Note that full information on the approval of the study protocol must also be provided in the manuscript.